Journal of Molecular Structure 1217 (2020) 128398

Contents lists available at ScienceDirect

Journal of Molecular Structure

journal homepage: http://www.elsevier.com/locate/molstruc

Two copper (II) complexes derived from anthranilic acid and 4-iodo-anthranilic acid Schiff bases: Structural elucidation, halogen bonding interactions and catalytic study using 3,5-DTBC

Barun Kumar Biswas [a], Sandeepta Saha [a, b], Niladri Biswas [a], Manas Chowdhury [a], Antonio Frontera [c], Corrado Rizzoli [d], Ruma Roy Choudhury [e], Chirantan Roy Choudhury [a, *]

[a] Department of Chemistry, West Bengal State University, Barasat, Kolkata 700126, India
[b] Sripur High School, Madhyamgram Bazar, Madhyamgram, Kolkata, 700130, India
[c] Departament de Química, Universitat de les Illes Balears, Crta. De Valldemossa km 7.5, 07122, Palma de Mallorca, Baleares, Spain
[d] Dipartimento S.C.V.S.A., University of Parma, Parco Area delle Scienze 17/A, 43124 Parma, Italy
[e] Department of Chemistry, Heritage Institute of Technology, Chowbaga Road, Anandapur, Kolkata, 700107, West Bengal, India

ARTICLE INFO

Article history:
Received 16 February 2020
Received in revised form
3 May 2020
Accepted 5 May 2020
Available online 10 May 2020

Keywords:
Copper
XRD
Catalyst
DFT
NCI plot

ABSTRACT

Two monomeric copper complexes [Cu(Pymab)(CCl_3COO)(H_2O)].H_2O (**1**) and [Cu(Pymaib)(H_2O)Cl]$_2$ (**2**) were synthesized by reacting copper (II) trichloroacetate and copper(II) chloride with the monobasic tridentate Schiff-Base ligands (HPymab = (E)-2-((pyridine-2-yl)methyleneamino)benzoic acid and HPymaib = 4-iodo-2-{(*E*)-[(pyridin-2-yl) methyleneamino}benzoic acid) and characterized by elemental analysis, IR, UV–Vis, mass spectrometry, CV and single crystal XRD analysis. Both complexes are monomeric in the solid state and in the solution as well. For both complexes, single crystal XRD indicates a distorted square pyramidal coordination geometry of the metal atoms. Both **1** and **2** behave as effective catalysts towards the oxidation of 3,5-di-*tert*-butyl catechol to the corresponding quinone derivative in aerial oxygen. The reactions follow the Michaelis-Menten enzymatic reaction kinetics with (k_{cat}) values of 1452 h^{-1} and 1458 h^{-1} respectively in DMSO and 1590 h^{-1} and 1636 h^{-1} in THF respectively. In the solid state both compounds participate in halogen bonding interactions that have been studied using DFT calculations and the molecular electrostatic potential (MEP) and the noncovalent interaction plot index (NCI plot) computational tools.

1. Introduction

For mimicking the structural property, or for reactivity study of biological metalloenzymes, biomimetic models are extensively designed [1]. For example, the copper-containing type-III metalloenzyme, catechol oxidase is responsible for the catalytic oxidation of catechols to quinones, which is called catecholase activity [2]. Being one of the essential micronutrients, copper is used by nature to play a crucial role in many biological processes [3], like oxygenation reaction, oxygen transport, electron transfer etc [4,5]. Because of the dinuclear copper(II) moiety present in the active site structure of catechol oxidase, dinuclear Copper(II) complexes having N–O donor ligands are the main focus of a number of studies [6–24]. Copper dimers easily oxidizes phenols and catechols and it is supported by various methods [25]. Besides dinuclear complexes, mononuclear copper (II) complexes are also able to show catecholase activity and follow different mechanisms [26,27]. From these reports, it is clear that for mononuclear complexes, when bulkiness around the central metal are less then K_{cat} values are high enough but the value becomes very low, when central metal ions are sterically crowded [28–31]. Mainly, two types of mechanisms are mentioned for the catalytic oxidation of substrates by these compounds [28–30]. So, study of newly synthesized model complexes having prominent catecholase activity and finding the correlation between structural and catalytic properties are considered as promising area of current day research [32]. Schiff bases are still one of the important types of coordinating ligands. Metal complexes with tridentate Schiff base ligands having N, N, O

* Corresponding author.
E-mail address: crchoudhury2000@yahoo.com (C. Roy Choudhury).

https://doi.org/10.1016/j.molstruc.2020.128398
0022-2860/

donor sites are employed for decoding the structural features of non-heme protenes [33,34]. In recent times, Schiff bases synthesized from pyridine 2-carboxaldehydes are widely studied because of its various possible applications in the field of chemotherapeutics and bio-mimetic catalysis on super oxide dismutase activities [35–46].

All these facts prompted us to synthesize two novel mononuclear copper (II) Schiff base complexes using pyridine-2-carboxaldehyde and anthranilic acid or 4-iodo-anthranilic acid respectively. The resulting complexes [Cu(Pymab)(CCl_3COO)(-H_2O)].H_2O (**1**) and [Cu(Pymaib)(H_2O)Cl]$_2$ (**2**) were evaluated for conversion of 3,5- DTBC to corresponding quinone. From the results it can be concluded that complexes **1** and **2** are very effective catalysts with k_{cat} values 1452 h^{-1} and 1458 h^{-1} respectively in DMSO and 1590 h^{-1} and 1636 h^{-1} in THF respectively.

2. Experimental section

2.1. Chemicals and methods

Anthranilic acid, 4-iodo-anthranilic acid, pyridine-2-carboxldehyde, cupric carbonate, copper(II) chloride were obtained from Sigma-Aldrich (USA). 3,5-di *tert*-butyl catechol, trichloroacetic acid were purchased from Spectrochem (India). All chemicals were used without further purification. All solvents were dried according to standard procedures and distilled before to use.

2.2. Physical characterization

Elemental analyses were performed on a PerkinElmer 2400 CHNS O element analyzer. Infrared spectra of complexes were recorded in the solid state as a KBr pellet on a PerkinElmer SPECTRUM Two FT-IR spectrophotometer within the range of 400–4000 cm^{-1}. Electronic spectra of **1** and **2** were recorded at 300 K on a PerkinElmer Lambda-35 UV–Vis spectrometer using DMSO as solvent. Cyclic voltammograms of **1** and **2** were recorded using CH-electrochemical analyzer with DMSO as solvent. We have done catecholase activity study by UV spectrometer (PerkinElmer Lamda-35) using 1 cm path length using the same solvent.

2.3. Synthesis

2.3.1. Synthesis of (Hpymab = (E)-2-((pyridine-2-yl) methyleneamino)benzoic acid)

Schiff base ligand HPymab was prepared according to literature method [47].

Anthranilic acid (0.137 g, 1 mmol) was dissolved in 20 ml of methanol and a solution of pyridine-2-carboxaldehyde (1 mmol) in 20 ml methanol were added dropwise to it with continuous stirring. The Schiff base ligand was prepared according to published procedure [47]. (Scheme 1A).

2.3.2. Synthesis of (HPmyaib = 4-iodo-2-{(E)-[(pyridin-2-yl) methyleneamino}benzoic acid)

Schiff base ligand (HPymaib) was prepared using the same method as HPymab using 4-iodo anthranilic acid (1 mmol) instead of anthranilic acid (Scheme-1B).

2.3.3. Preparation of copper trichloroacetate

Copper trichloro acetate was prepared using the standard literature procedure [48].

2.3.4. Synthesis of [Cu(Pymab)(CCl_3COO)(H_2O)].H_2O (**1**)

A methanolic solution (20 ml) of Copper (II) trichloroacetate (0.390 g, 1 mmol) was taken in a 100 ml beaker, then 20 ml of *HPymab* (1 mmol) was added dropwise to it. After addition of *HPymab* the solution turned blue to light green. Then, the solution was stirred for 5 min over a magnetic stirrer. Then the solution was filtered and left for crystallization. After a weak, green coloured crystals (yields ~ 65%) separated out and it was used for characterization.

Yield: 65% (0.360 g), Anal. Calc. For [$C_{15}H_{11}Cl_3CuN_2O_5 \cdot H_2O$] (**1**) C, 36.94; H, 2.67; N, 5.74%. Found: C, 36.91; H, 3.59; N, 5.67%. IR (KBr, cm^{-1}): 1691(s), 1568-1586(s), 1324-1363(s) and 743-778(b).

2.3.5. Synthesis of [Cu(Pymaib)(H_2O)Cl]$_2$ (**2**)

Complex **2** was synthesized using Copper (II) chloride instead of Copper (II) trichloroacetate and HPymaib instead of HPymab (1 mmol) by the same procedure as in complex **1**.

Yield: 67% (0.315 g), Anal. Calc. For [$C_{13}H_{10}ClCuIN_2O_3$] (**2**) C, 33.32; H, 2.14; N, 5.98%. Found: C, 33.22; H, 2.18; N, 5.89%. IR (KBr, cm-1): 1685(s), 1582-1592(s), 1444-11490(s) and 749-741(b).

2.4. Single-crystal X-ray diffraction study

Good quality single crystals of **1** and **2** were mounted on a Bruker APEX2 CCD diffractometer respectively, equipped with graphite monochromatized Mo $K\alpha$ radiation (λ = 0.71073 Å) fine-focus sealed tubes. Intensity data were collected at 294 K using ω scans. Crystal data of both complexes were collected using Apex2

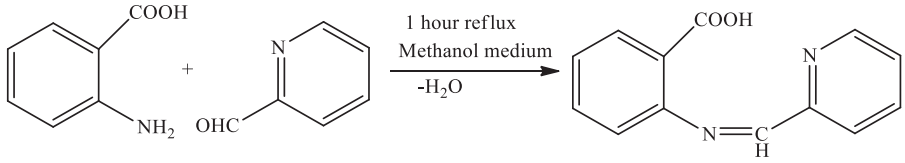

A

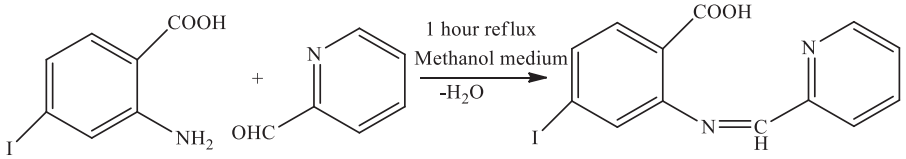

B

Scheme 1.

[41]. Data refinement and reduction were performed using SAINT (Bruker, 2008) [41]. Multiscan absorption corrections were applied empirically to the intensity values (T_{min} = 0.334 and T_{max} = 0.745 for **1** and T_{min} = 0.581 and T_{max} = 0.746 for **2**) using SADABS [49]. The structures were solved by direct methods using the program SHELXT [42a,50a] for **1** and **2**, and refined with full-matrix least-squares based on F^2 using program SHELXL-2014/7 [50b] for the complexes. All non-hydrogen atoms were refined anisotropically. In both complexes the water H-atoms were placed in chemically sensible positions on the basis of hydrogen bonding interactions and refined with $U_{iso}(H) = 1.5U_{eq}(O)$. The O—H bond lengths and H···H separations were constrained to 1.30(1) and 0.82(1) Å, respectively. The minimum H···H separation between the independent water molecules was also constrained to be 2.20(1) Å. All other H atoms were placed geometrically and refined using a riding atom approximation, with C—H = 0.93 Å, and with $U_{iso}(H) = 1.2U_{eq}(C)$. The molecular graphics and crystallographic illustrations for **1** and **2** were prepared using Olex2 [51a] POV ray [51b] and ORTEP 3 [52] programs. Crystallographic data and structure refinement parameters for **1** and **2** are summarized in Table 1.

2.5. Theoretical methods

The energetic and geometric features of the complexes included in this study were calculated at the B3LYP-D3/def2-TZVP level of theory using the crystallographic coordinates (only the positions of the H-atoms were optimized). For the calculations, the GAUSSIAN-16 program has been used [53]. The basis set superposition error for the calculation of interaction energies has been corrected using the counterpoise method [54]. Molecular electrostatic potential (MEP) surfaces have been computed at the same level of theory and represented using the 0.001 a.u. isosurface. The NCI plot index [55] computational tool has been used to characterize non-covalent interactions using the B3LYP-D3/def2-TZVP level wave function. They correspond to both favorable and unfavorable interactions, as differentiated by the sign of the second density Hessian eigen value and defined by the isosurface color. The color scheme is a red-yellow-green-blue scale with red for ρ^{+}_{cut} (repulsive) and blue for ρ^{-}_{cut} (attractive). Yellow and green isosurfaces correspond to weakly repulsive and attractive interactions, respectively.

3. Results and discussion

3.1. Synthetic pathway of complex formation

Copper(II) complexes were prepared by the reaction of copper trichloroacetate and copper chloride with methanolic solution of NNO donor Schiff base ligands *HPymab* and *HPymaib* respectively in 1:1 M proportions. The details pathway is given in Scheme 2A (Complex **1**) and Scheme 2B (Complex **2**). Both the complexes **1** and **2** possess distorted square pyramidal geometry and are stable in air at room temperature. Complexes **1** and **2** are characterised by IR, UV—Vis spectroscopy, cyclic voltammetry and single crystal X-ray crystallography. All the spectroscopic data are consistent with the crystal structures of the complexes **1** and **2** discussed in this paper.

3.2. IR spectral study

IR Spectra of **1** and **2** are shown in Figs. S1A and S1B respectively. Both complexes exhibit strong bands in the region of 1691 cm^{-1} and 1685 cm^{-1} respectively, due to presence of $\nu_{(C=N)}$ [56]. Broad peaks due to $\gamma_{(N-H)}$ wagging are observed at around 743-778 cm^{-1} and 749-741 cm^{-1} respectively [17]. Both complexes showed ν_{assym} (COO^-) and ν_{sym} (COO^-) peaks due to the presence of carboxylate ions. Due to the presence of carboxylate groups, ν_{assym} (COO^-) [1568-1586 and 1582-1592 cm^{-1}] and ν_{sym} (COO^-) [1324-1363 and 1444-1490 cm^{-1}] peaks are observed [57—59]. The large difference between the two bands indicates the monodented nature of the active group [57—59].

3.3. Electronic spectral study

Electronic spectra of the complexes **1** and **2** were recorded in DMSO and display (Figs. S2A and S2B) board absorption bands at 740 and 709 nm respectively, which are in agreement with the *d*-

Table 1
Crystallographic data and structural refinement of complexes **1** and **2.**

	1	2
empirical formula	$C_{15}H_{11}Cl_3CuN_2O_5 \cdot H_2O$	$C_{13}H_{10}ClCuIN_2O_3$
formula weight (g mol^{-1})	487.16	468.12
temperature	294	294
crystal system	Monoclinic	Triclinic
space group	$P2_1/c$	*P-1*
a (Å)	14.173(8)	9.2267(16)
b (Å)	9.830(6)	9.3259(16)
c (Å)	13.642(8)	18.008(3)
α (deg)	90	87.333(2)
β (deg)	106.298(5)	89.982(3)
γ (deg)	90	77.508(3)
V(Å^3)	1824.2(19)	1511.1(4)
Z	4	4
d_{calc} (g cm^{-3})	1.774	2.058
μ (mm^{-1})	1.673	3.674
F(000)	980	900
crystal size (mm^3)	0.07 × 0.17 × 0.22	0.03 × 0.06 × 0.15
θ range (deg)	1.5—25.2	1.1—25.2
measured reflections	3270	5430
independent reflections	2196	4682
R(int)	0.087	0.031
goodness-of-fit on F^2	1.050	1.039
final *R* indices[I > 2σ(I)]	R_1 = 0.0786, wR_2 = 0.1979	R_1 = 0.0527, wR_2 = 0.1678 w*R*2 = 0.1063
R indices (all data)	R_1 = 0.1122, wR_2 = 0.2196	R_1 = 0.0590, wR_2 = 0.1736 w*R*2 = 0.0984
$\Delta\rho_{min}$ and $\Delta\rho_{max}$ (e Å^{-3})	−0.75 and 0.98	−1.45 and 2.53

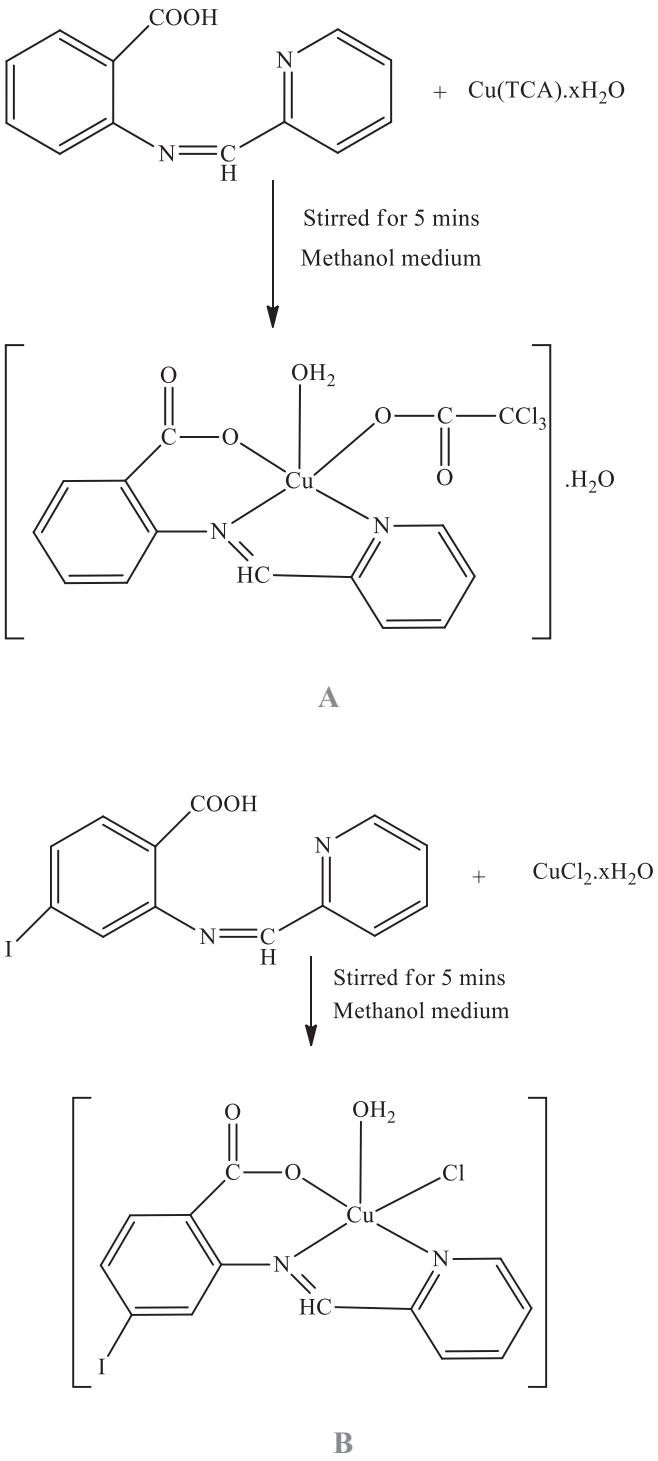

Scheme 2. A (Synthesis of Complex **1**). **B** (Synthesis of Complex **2**).

d transition bands of copper (II) [60]. Two higher energy bands appeared in the spectra at 341, 260 nm and 333, 252 nm for complexes **1** and **2** respectively, which are assigned for n to π* and π to π* transitions respectively. .

3.4. Cyclic voltammetry

Electrochemical study was carried out for complexes **1** and **2** in Tris-HCl buffer medium under nitrogen atmosphere in the potential range from +2.0 to −2.0 V using tetrabutylammonium perchlorate as supporting electrolyte. The voltammograms of complexes **1** and **2** are shown in Fig. 1. In both complexes one prominent oxidative peak is observed at 0.85 and 0.77 V for **1** and **2**, respectively which corresponds to Cu(II) to Cu(III) oxidation. Fig. 1 shows reduction peaks for **1** and **2** with cathodic wave potential −0.44 and −0.56 V, respectively corresponding to the Cu(II) to Cu(I) redox couple.

3.5. X-ray crystal structure description

3.5.1. Crystal structure of *1*

A thermal ellipsoid drawing of the structure of complex **1** indicating atom numbering scheme is shown in Fig. 2. Selected bond lengths and bond angles are given in Tables 2a and 2b. The complex crystallizes as a five-coordinate monomeric species. The copper(II) ion adopts a distorted square pyramidal geometry ($\tau = 0.23$) [61] with the donor atoms forming the basal plane being the pyridine nitrogen atom (N1), the imine nitrogen atom (N2) and the carboxylate oxygen atom from anthranilic acid part (O1) of the Schiff base H*Pymab* plus the oxygen (O3) from the trichloroacetate anion. One water molecule coordinates weakly in the apical site through (O5).

The Schiff base is coordinated to the copper(II) ion in its iminocarboxylate form. While coordinating in this form, the negative charge generated upon deprotonation of the COOH proton is delocalized across the six membered ring Cu1/O1/C13/C12/C7/N2 as indicated by the intermediate value of C7—N2 {1.431(4) Å} and C12—C13 bond distances {1.520 Å}. These bonds may be compared with the well with those of the analogous five-coordinate square-pyramidal copper(II) complex, {[Cu(Pymab)(H_2O)](NO_3)}$_4$ [47,62], whose structure has been elucidated by X-ray diffraction. The geometry of the complex is distorted square-pyramidal conceivably as a consequence of the restricted bite of the tridentate Schiff base ligand. The five- and six-membered chelation rings are approximately planar (r.m.s. deviation is 0.0115 and 0.0914 for rings Cu1/N1/C5/C6/N2 and Cu1/N2/C7/C12/C13/O1), the mean planes through them forming a dihedral angle of 13.40(15)°.In the crystal the complex molecules and the water molecules of crystallization are linked by classical O—H···O, nonclassical C—H···O and C—H···Cl hydrogen bonds into a three-dimensional network (Fig. 3, Table S3A). Cohesion of the crystal structure is further stabilized by π … π stacking interactions (centroid-to-centroid distance 3.646(5) Å) occurring between the benzene and pyridine rings of adjacent molecules.

3.5.2. Crystal structure of *2*

The asymmetric unit of **2** (Fig. 4) contains two independent mononuclear complexes having similar conformation. An overlay of structures of the independent complexes is shown in Fig. 5. For sake of simplicity the molecule containing atom Cu1 and Cu2 will be hereafter referred as molecule *A* and *B* respectively. The copper(II) metals are five-coordinated by the N, O and Cl donor atoms of a tridentate HPymaib ligand, a water molecule and a chloride anion. Based on the trigonality index τ [61], which assumes a value of 0.0 and 1.0 for ideal square pyramidal and trigonal bipyramidal geometries, the coordination geometry about the copper(II) metal in *A* can be described as distorted square pyramid ($\tau = 0.205$), whereas a somehow more regular square pyramidal coordination geometry is observed in *B* ($\tau = 0.16$). In both coordination geometries the basal plane is provided by the N and O atoms and the apical position is occupied by the chloride anion. The 5-membered chelate ring is approximately planar in both molecules (r.m.s. deviation is 0.274 and 0.0144 Å for rings Cu1/N1/C5/C6/N2 and Cu2/N3/C18/C19/N4, respectively). The six-membered chelate rings

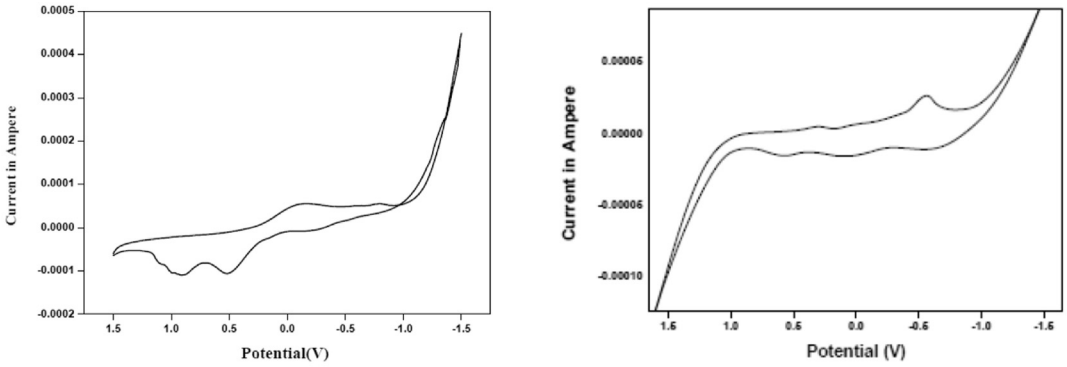

(a) (b)

Fig. 1. (a): Cyclic voltammogram of complex **1**, (b) Cyclic voltammogram of Complex **2.**

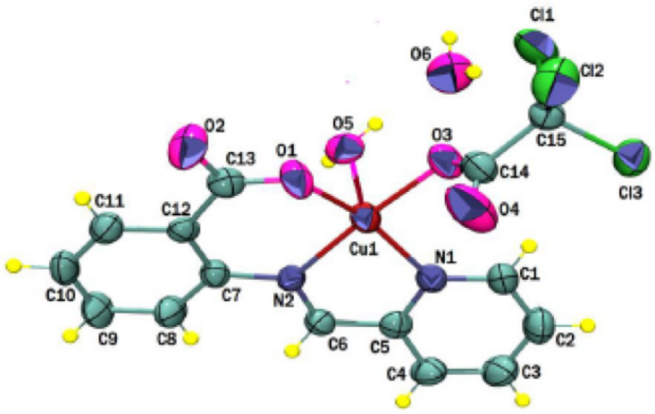

Fig. 2. Crystal Structure of Complex **1** with displacement ellipsoids drawn at the 50% probability level.

assume an envelope conformation, with atoms Cu1 and Cu2 displaced by 0.8363(8) and 0.7290(8) Å respectively from the mean plane through the rest of the rings. In *A* and *B* the dihedral angle between the mean planes through the five- and six-membered rings is 34.75(13) and 38.88(13)°, respectively, and the benzene ring is oriented with respect to the pyridine ring to form a dihedral angle of 37.9(2) and 24.8(2)° respectively. Bond distances (Table 2a) and angles (Table 2b) are unexceptional and in agreement with those observed in related compounds [63].

It was observed that often molecules related to **2** form centrosymmetric dimers via Cu–X bridges (X = halogens or pseudo halogens) [64]. In **2**, dimeric units are generated through classical hydrogen bonds involving the water molecule and the carboxyl group of molecule *A* and the water molecule and the chloride anion of molecule *B* (Table S3B). The Cu···Cu separation within the dimeric unit is 5.7069(13) Å. In the crystals, the dimers are further linked into layers parallel to the *ab* plane (Fig. 6) through O–H···O, O–H···Cl and C–H···Cl hydrogen interactions.

3.6. Catecholase activity of complexes *1* and *2*

For the study of the catecholase activity of complexes **1** and **2**, 3,5-DTBC, with two bulky *tert*-butyl substituents on the ring and low quinine-catechol reduction potential, has been chosen as the substrate [65]. In the presence of bulky substituent, further oxidation and polymerization are stopped. Both **1** and **2** exhibit extensive catalytic competence toward the oxidation of 3,5 –DTBC to 3,5- DTBQ in the solvent DMSO and THF [66]. This catecholase reaction was investigated using UV–Vis spectroscopy studies in DMSO and THF solutions (as illustrated in Scheme 3) [67]. To perform the kinetic studies, 1×10^{-4} mol dm^{-3} solutions of **1** and **2** were added to 100 equivalent of the substrate in DMSO or in THF under aerobic condition at 25 °C [68]. The time dependent UV–Vis spectral scan was executed after addition of catalyst **1** at 5 min time intervals up to 90 min for complex **1** and 70 min for complex **2**. As the reaction progressed, new bands at ~392 nm for complex **1** and 390 nm for complex **2** were generated which clearly indicate the formation of corresponding quinone derivative 3,5-DTBQ [Figs. 7 and 8]. When THF were used as solvent, new bands at ~394 nm for complex **1** and 396 nm for complex **2** were generated which clearly indicate the formation of corresponding quinone derivative 3,5-DTBQ [Figs. 9 and 10].

The kinetics of the oxidation of 3,5-DTBC was determined by the method of initial rates by monitoring the growth of the product 3,5-DTBQ, the experimental conditions were the same as reported

Table 2a
Selected bond lengths (Å) for **1** and **2**.

Complex 1		Complex 2	
Cu1–O1	1.916(5)	Cu1–Cl1	2.252(2)
Cu1–O3	1.955(6)	Cu1–O1	2.007(6)
Cu1–O5	2.265(6)	Cu1–N1	2.162(6)
Cu1–N1	2.005(5)	Cu1–N2	2.132(5)
Cu1–N2	2.009(6)	Cu1–O3	2.002(6)
		Cu2–N3	2.132(6)
		Cu2–N4	2.165(5)
		Cu2–O6	2.016(6)
		Cu2–Cl2	2.256(2)
		Cu2–O4	1.986(5)

Table 2b
Selected bond angles (°) for **1** and **2**.

Complex 1		Complex 2	
O1–Cu1–O3	92.2(2)	Cl1–Cu1–O1	109.20(19)
O1–Cu1–O5	95.9(2)	Cl1–Cu1–O3	109.92(18)
O1 –Cu1–N1	162.0(2)	Cl1–Cu1–N1	113.62(16)
O1–Cu1–N2	91.7(2)	Cl1–Cu1–N2	102.18(16)
O3–Cu1–O5	88.6(2)	O1–Cu1–O3	85.2(2)
O3 –Cu1 –N1	93.5(2)	O1–Cu1–N1	135.6(2)
O3–Cu1–N2	175.6(2)	O1–Cu1–N2	83.7(2)
O5–Cu1–N1	101.3(2)	O3–Cu1–N1	90.9(2)
O5–Cu1–N2	92.9(2)	O3–Cu1–N2	147.9(2)
N1–Cu1–N2	82.2(2)	N1–Cu1–N2	76.6(2)
		O4–Cu2–O6	85.1(2)
		O4–Cu2–N3	138.3(2)
		O4–Cu2–N4	84.73(18)
		Cl2–Cu2–O4	112.22(17)
		Cl2–Cu2–O6	108.00(18)
		Cl2–Cu2–N3	108.39(18)
		Cl2 –Cu2–N4	104.03(15)
		O6–Cu2–N3	91.2(2)
		O6–Cu2–N4	147.9(2)
		N3–Cu2–N4	76.8(2)

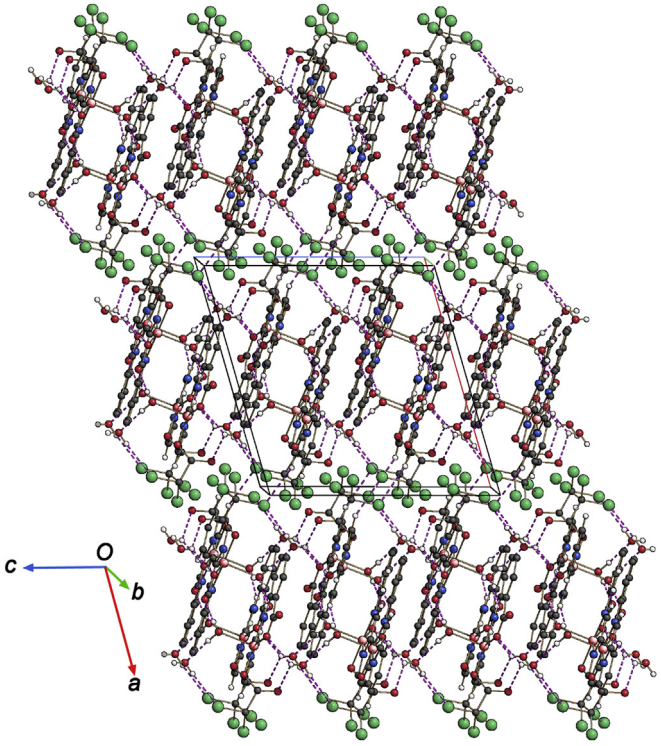

Fig. 3. Crystal packing of complex **1** approximately viewed down the *b* axis, showing the three-dimensional hydrogen-bonding network (dashed lines). Hydrogen atoms not involved in hydrogen bonds are omitted.

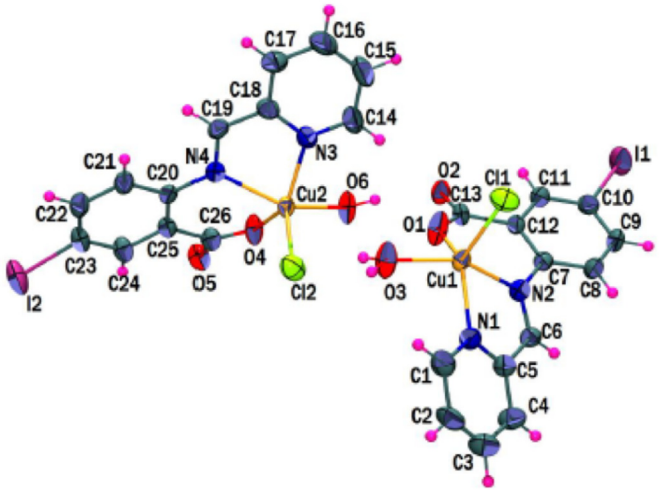

Fig. 4. Crystal Structure of Complex **2** with displacement ellipsoids drawn at the 50% probability level.

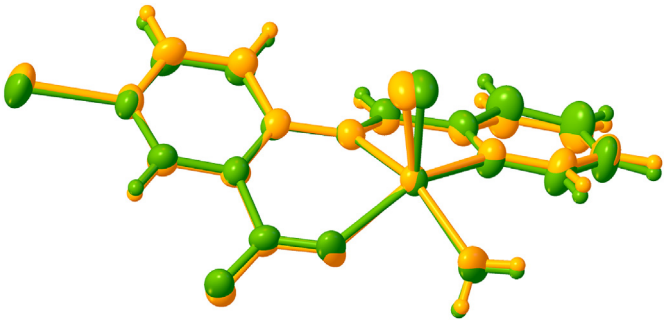

Fig. 5. Overlay diagram of the two independent molecules in complex **2** (1) (yellow image contains Cu1).

earlier [67,69–71].

The kinetic parameters were determined by applying the Michaelis-Menten approach and the results were obtained from Lineweaver-Burk plots [68]. The binding constant (k_m), maximum velocity (V_{max}) and rate constant for the conversion of the substrate (turnover number, K_{cat}) were calculated for both complexes **1** and **2** in solvents DMSO and THF respectively, using the Lineweaver-Burk graph of 1/v *vs.* 1/[s], using equation $1/v = \{ K_M/V_{Max}(1/[s]) \; 1/V_{Max} \}$ [36] [Figs. 11a, b and 12a, b] for DMSO solvent and [Figs. 13a, b and 14a, b] for THF solvent. The kinetic parameters V_{max} and K_{cat} of the complexes **1** and **2** are listed in Table 3.

From the data presented in Table 4 it may be inferred that the catalytic efficiency of **1** and **2** in both the DMSO and THF solvent are nearly comparable with copper catalysts [72–79]. From the kinetic data, it is observed that K_{cat} value of complex **2** is slightly higher than that of complex **1.** Rate constants for the oxidation of catechols

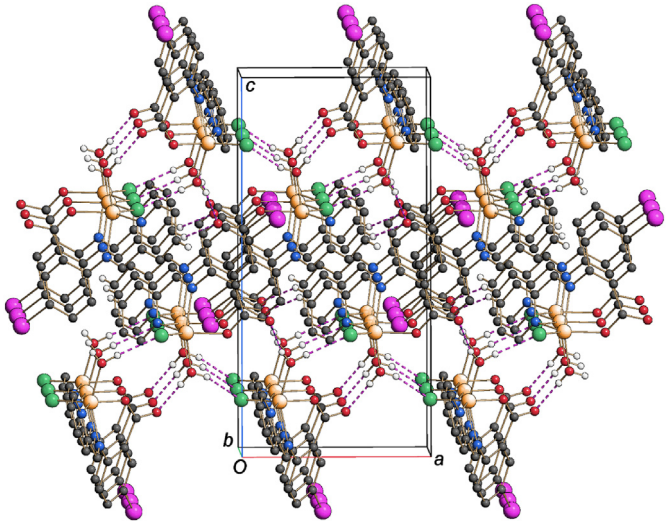

Fig. 6. Crystal packing of **2** approximately viewed along the *b* axis showing the hydrogen bonding network (dashed lines).

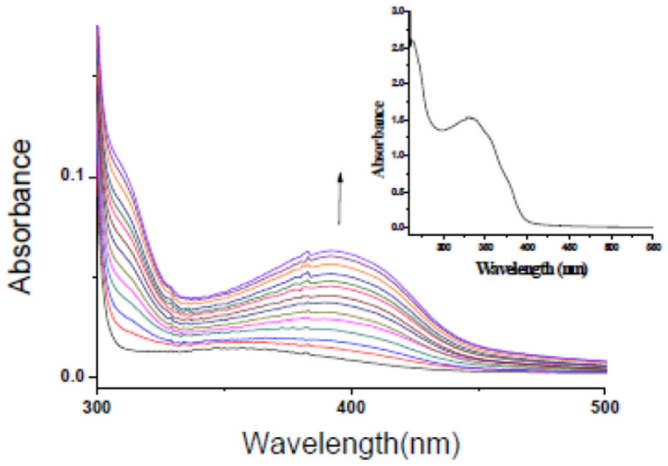

Fig. 8. Change in Spectral pattern of complex **2** after reaction with 3,5- DTBC, Observing the reaction for 70 Min in DMSO: Inset UV–Vis spectrum for complex **2** in DMSO.

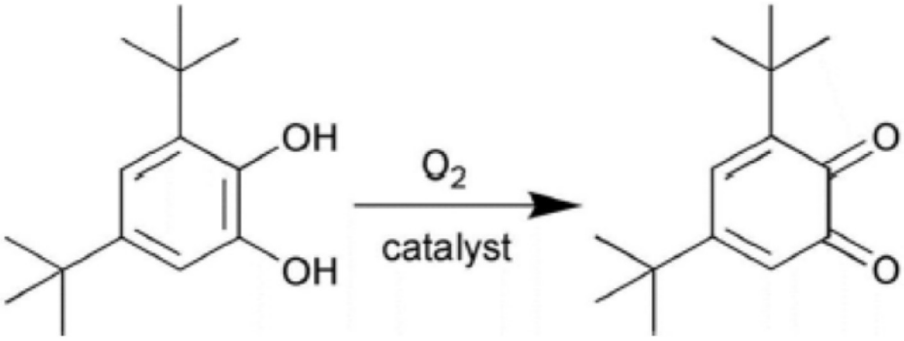

Scheme 3. Oxidation of 3,5-DTBC to 3,5-DTBQ.

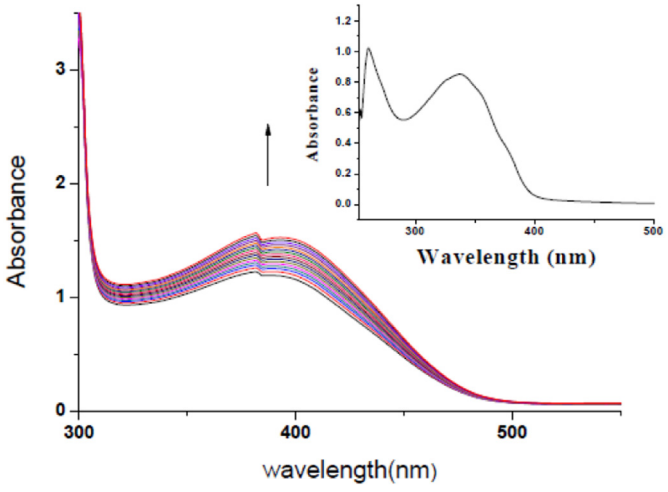

Fig. 7. Change in Spectral pattern of complex **1** after reaction with 3,5- DTBC, Observing the reaction for 90 min in DMSO: Inset UV–Vis spectrum for complex **1** in DMSO.

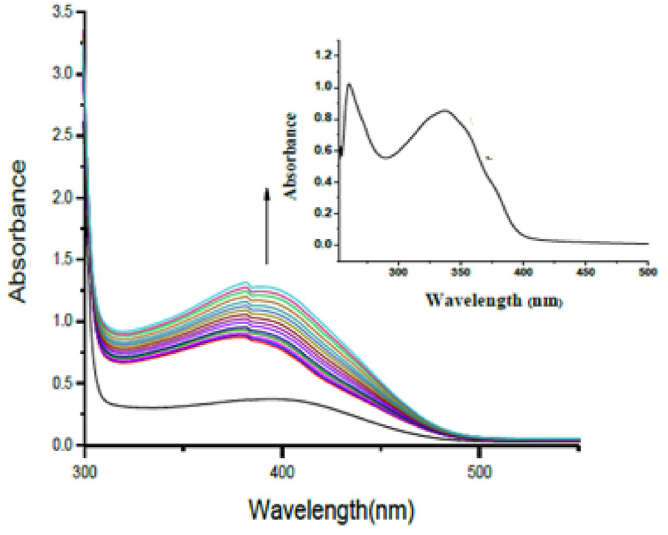

Fig. 9. Change in Spectral pattern of complex **1** after reaction with 3,5- DTBC, observing the reaction for 90 min in THF. Inset UV–Vis spectrum for complex **1** in THF.

by complexes **1** and **2** with similar previously reported Cu(II), Ni (II), Mn (II/III) and Zn (II) complexes using 3,5-DTBC as the substrate are given in Table 4.

Some mononuclear and dinuclear copper (II) complexes can be correlated [80–83]. This type of correlation of relative activity is usually depends on the Cu···Cu distance [81a,83a], coordination geometry around metal centre [82c,82d], nature of the substituents

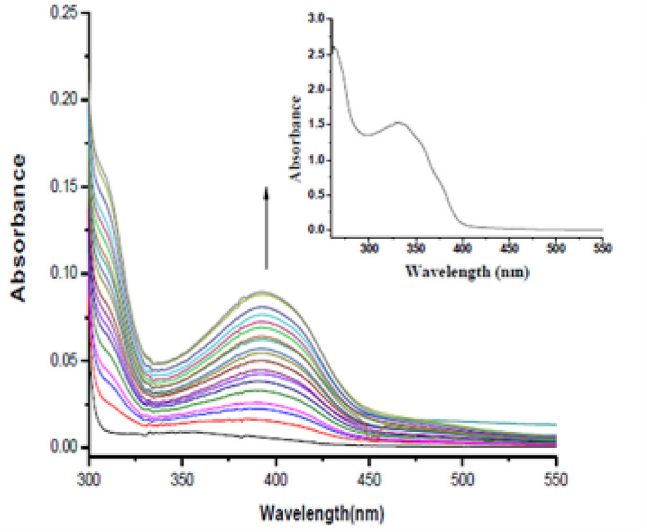

Fig. 10. Change in Spectral pattern of complex **1** after reaction with 3,5- DTBC, observing the reaction for 90 min in THF. Inset UV–Vis spectrum for complex **1** in THF.

of the ligands [83b] and steric strain of the compounds [83b]. Another correlation for mononuclear manganese(III) catalysts is described where the role of the apical ligand on the activity has been discovered [84].

3.7. Mechanism of catalytic oxidation of 3,5 DTBC with complex *1* or *2*

A plausible mechanism for catalysis of 3,5- DTBC by complex **1** or **2** are provided in Scheme 4. It may be suggested that in the first step $DTBCH_2$ displace $-H_2O$ and $-OCOCCl_3$/-Cl from the coordination sphere and gets attached with complex **1** or **2**. So in this case $DTBC^{2-}$ is coordinated as a bidented ligand. A semi-quinone is formed when $DTBC^{2-}$ provide one electron and consequently semiquinone complex possess Cu^{I}-central metal ion. Cu^{I} – complex readily reacts with available O_2 from air and form Cu^{II}-superoxo species, involving semi quinone ligand. Next step would be regeneration of catalyst and elimination of H_2O_2 (Figs. S4 and S 5 Supplementary information) [32,73,85–87]. For the detection of H_2O_2 during catalytic oxidation modified iodometric method was applied [27,88]. Formation of H_2O_2 was confirmed by detection of I_3^- band at 353 nm by UV–Vis spectroscopy [2,27].

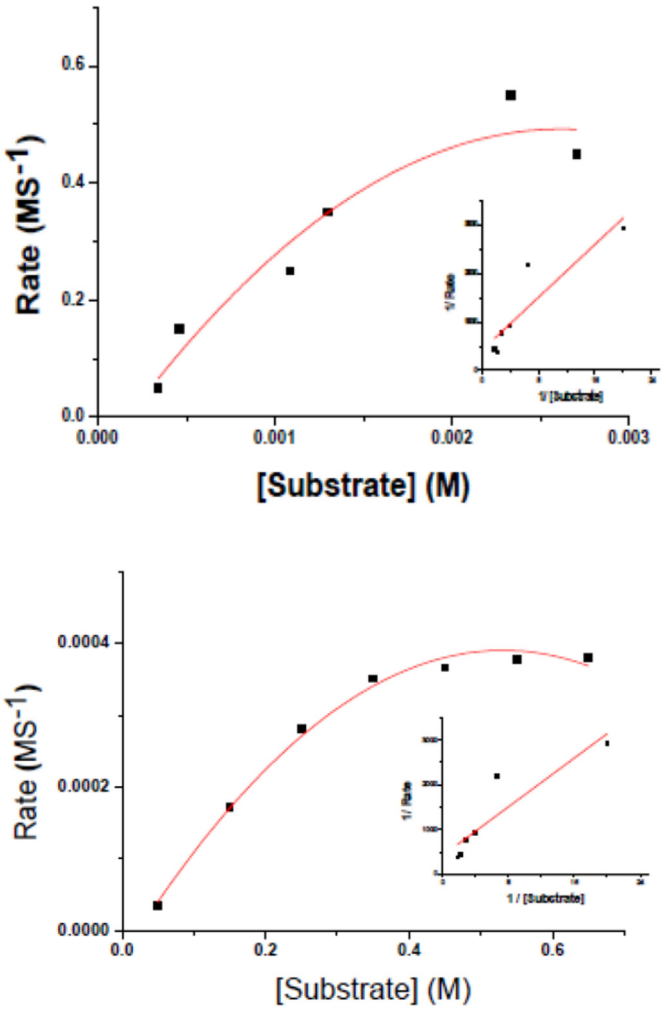

Fig. 12. a. Plot of rate *vs.* [substrate] (3,5-DTBC) in presence of complex **1** in DMSO; Inset: Lineweaver-Burk plot. **12 b**. Plot of rate *vs.* [substrate] (3,5-DTBC) in presence of complex **2** in DMSO; Inset: Lineweaver-Burk plot.

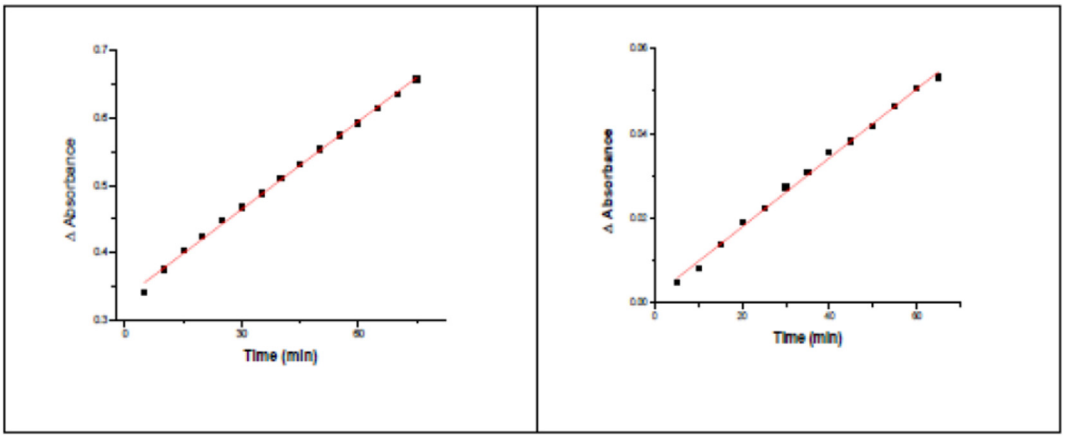

Fig. 11. (a)A plot of the difference in absorbance (ΔA) *vs.* time to evaluate the rate of catalysis of 3,5-DTBC by complex **1** in DMSO; (b) A plot of the difference in absorbance (ΔA) *vs.* time to evaluate the rate of catalysis of 3,5-DTBC by complex **2** in DMSO.

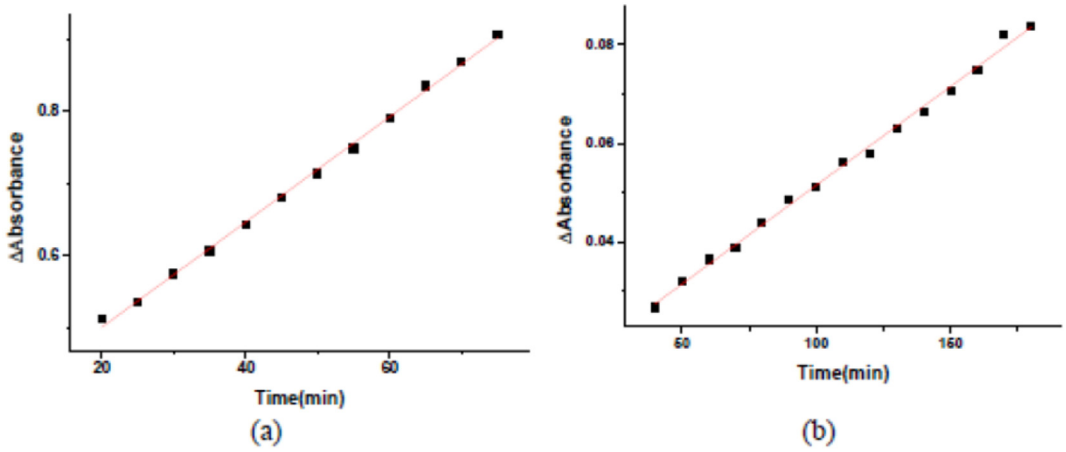

Fig. 13. (a)A plot of the difference in absorbance (ΔA) *vs*. time to evaluate the rate of catalysis of 3,5-DTBC by complex **1** in THF; (b) A plot of the difference in absorbance (ΔA) *vs*. time to evaluate the rate of catalysis of 3,5-DTBC by complex **2** in THF.

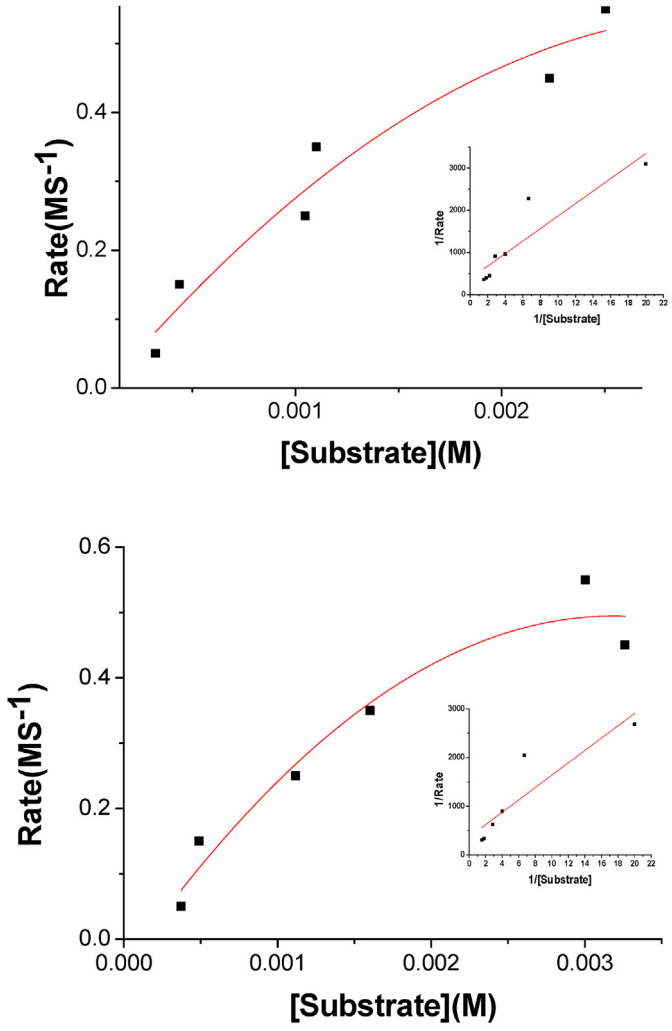

Fig. 14. a. Plot of rate *vs*. [substrate] (3,5-DTBC) in presence of complex **1** in THF; Inset: Lineweaver-Burk plot. **b.** Plot of rate *vs*. [substrate] (3,5-DTBC) in presence of complex **2** in THF; Inset: Lineweaver-Burk plot.

Table 3
The kinetic parameters for the catalytic oxidation of 3,5-DTBC mediated by complexes **1** and **2**.

Complexes	Solvent	V_{max} (MS^{-1})	K_M (M)	K_{cat} (h^{-1})
1	DMSO	24.20×10^{-4}	32.94×10^{-2}	1452.00
2	DMSO	24.30×10^{-4}	33.10×10^{-2}	1458.00
1	THF	26.50×10^{-4}	39.33×10^{-2}	1590.00
2	THF	27.26×10^{-4}	34.62×10^{-2}	1636.00

3.8. Theoretical study

The theoretical DFT study is devoted to analyze the halogen bonding interactions observed in the solid state of both compounds **1** and **2**, as detailed below. We have first computed the molecular electrostatic potential (MEP) of both compounds in order to examine electron rich and electron poor regions of the molecule, paying special attention to the existence of a σ-hole at the extension of the C—X bonds (X = Cl, I). The MEP surfaces are shown in Fig. 15 for both compounds. The most positive MEP value in compound **1** is located at the coordinated water molecule and the most negative at the carboxylate groups of the ligands. At the extension of the C—Cl bond the MEP value is slightly positive, thus indicating a very small sigma hole. This is likely due to the anionic nature of the trichloroacetate ligand. In contrast for compound **2**, the MEP value at the extension of the C—I bond is large and positive (+16 kcal/mol), thus more suitable for establishing halogen bonding interactions. This behavior is typical in halogen bonding that is favored for the heavier halogen atoms. In**2**, the most negative potential is located at the carboxylate group and chlorido ligand.

In Fig. 16a we show a dimer of compound **1** retrieved from its X-ray packing where it can be observed the formation of a quite directional C—Cl···O halogen bond. We have evaluated the dimerization energy that is moderately strong, $\Delta E_1 = -9.1$ kcal/mol. It is worth mentioning that the coordinated water molecule of one complex (highlighted in yellow in Fig. 16a) is located at 3.26 Å from the one O-atom of the coordinated carboxylate group. Since both groups (water and carboxylate) are, according to the MEP in Fig. 15a, the most positive and negative regions of the molecule, the interaction energy could be influenced by this long distance H-bond (electrostatically enhanced). Consequently, we have computed a theoretical model where this water molecule has been eliminated and the interaction energy is reduced to $\Delta E_2 = -3.4$ kcal/mol, that corresponds to the contribution of the

Table 4
First order rate constant for the oxidation of catechols by complexes **1** and **2** with similar previously reported Cu(II), Ni (II), Mn (II/III) and Zn (II) complexes using 3,5-DTBC as the substrate.

Complexes	Solvent	Metal Present	Oxidation state	K_{cat} (in h^{-1})	Ref.
$[Cu(Pymab)(CCl_3COO)(H_2O)].H_2O$ (1)	DMSO	Cu	(II)	1452.00	This work
	THF	Cu	(II)	1590.00	
$[Cu(Pymaib)(H_2O)Cl]_2$ (**2**)	DMSO	Cu	(II)	1458.00	This work
	THF	Cu	(II)	1636.00	
$[Cu_2(H_2L2^2)(OH)(H_2O)(NO_3)](NO_3)_3\cdot 2H_2O$[b]	MeOH	Cu	(II)	32400	[65]
$[Cu(HL1^4)(H_2O)(NO_3)]_2(NO_3)_2\cdot 2H_2O$[b]	MeOH	Cu	(II)	14400	[65]
$[Cu(L1^1)(H_2O)(NO_3)]_2^b$	MeOH	Cu	(II)	10800	[65]
$[Cu_2(L2^3)(OH)(H_2O)_2](NO_3)_2^b$	MeOH	Cu	(II)	14400	[65]
$[Cu_2(L2^1)(N_3)_3]^b$	MeOH	Cu	(II)	28800	[65]
$[Cu_2(L1^1)(OH)(H_2O)(NO_3)_2]^c$	DMSO	Cu	(II)	73.70	[66]
$[Cu_2(L1^2)(OH)(H_2O)(NO_3)_2]^c$	DMSO	Cu	(II)	50.50	[66]
$[Cu(L2^1)(H_2O)(NO_3)]_2^c$	DMSO	Cu	(II)	84.60	[66]
$[Cu_2(L1^3)(OH)(H_2O)(NO_3)_2]^c$	DMSO	Cu	(II)	127.20	[66]
$[Cu_2(L1^4)(OH)(H_2O)(NO_3)_2]^c$	DMSO	Cu	(II)	49.60	[66]
$[Cu_2(L1^5)(OH)(H_2O)(NO_3)_2]^c$	DMSO	Cu	(II)	246.80	[66]
$[Cu_2(L1^6)(OH)(H_2O)(NO_3)_2]^c$	DMSO	Cu	(II)	50.70	[66]
$[Cu_2(L1^7)(OH)(H_2O)_2(NO_3)_2]^c$	DMSO	Cu	(II)	26.90	[66]
$[Cu_2(L1^9)(OH)(H_2O)(NO_3)_2]^c$	DMSO	Cu	(II)	51.80	[66]
$[Cu_2(L1^{10})(OH)(H_2O)(NO_3)_4]^c$	DMSO	Cu	(II)	68.30	[66]
$[Cu_2(L1^{12})(OH)(H_2O)(NO_3)_2]^c$	DMSO	Cu	(II)	50.10	[66]
$[Cu_2(Sgly)_2(H_2O)]$ $2H_2O$	MeOH	Cu	(II)	563	[67]
$[Cu_2(D\text{-}Sala)_2(H_2O)]$ H_2O	MeOH	Cu	(II)	564	[67]
$[Cu_2(L\text{-}Sala)_2(H_2O)]$ H_2O	MeOH	Cu	(II)	666	[67]
$Cu_2(D,L\text{-}Sala)_2(H_2O)_2]$ $2H_2O$	MeOH	Cu	(II)	365	[67]
$[Cu_2(Sab2)_2(H_2O)_2]$	MeOH	Cu	(II)	564	[67]
$[Cu_2(Sbal)_2(H_2O)_2]$	MeOH	Cu	(II)	1287	[67]
$[Cu_2(Sab4)_2(H_2O)_2]$ $0.5H_2O$	MeOH	Cu	(II)	3800	[67]
$[Cu_2(Sval)_2(H_2O)_3]$	MeOH	Cu	(II)	678	[67]
$[Cu_2(Shis)_2(H_2O)]$ H_2O	MeOH	Cu	(II)	244	[67]
$[Cu_2(Styr)_2(H_2O)]$ $2H_2O$	MeOH	Cu	(II)	265	[67]
$[Cu_2(Stryp)_2(H_2O)]$	MeOH	Cu	(II)	199	[67]
$[NiL^1(H_2O)_3]I_2\cdot H_2O$[a]	MeOH	Ni	(II)	9.27	[68]
$[NiL^1(H_2O)_3]Br_2\cdot H_2O$[a]	MeOH	Ni	(II)	8.48	[68]
$[MnL^1(OOCH)(OH_2)]^e$	MeCN	Mn	(II)	936.64	[69a]
$[MnL^2(OH_2)_2][Mn_2(L_2^2(NO_2)_3]^e$	MeCN	Mn	(II)	365.34	[69a]
$[Mn_2L_2(NO2)_2]^e$	MeCN	Mn	(II)	1432.74	[69a]
$[MnL^2Cl\cdot 4H_2O]^f$	MeOH	Mn	(II)	247.00	[69b]
$[MnL^3Cl\cdot 4H_2O]^f$	MeOH	Mn	(II)	360.00	[69b]
$[MnL^4Cl\cdot 4H_2O]^f$	MeOH	Mn	(II)	720.00	[69b]
$[Mn_2^{IV}(L_A^1)_2(L^{1\bullet})]^g$	CH_2Cl_2	Mn	(IV)	12.60	[70]
$[Mn^{IV}(L_A^2)(L^{2\bullet})_2]^g$	CH_2Cl_2	Mn	(IV)	21.30	[70]
$[Mn^{IV}(L_A^3)(L^{3\bullet})_2]^g$	CH_2Cl_2	Mn	(IV)	55.20	[70]
$[Mn^{IV}(L_A^4)(L^{4\bullet})_2]^g$	CH_2Cl_2	Mn	(IV)	14.80	[70]
$[Mn^{IV}(L_A^5)(L^{5\bullet})_2]^g$	CH_2Cl_2	Mn	(IV)	34.14	[70]
$[Mn^{IV}(L_A^6)(L^{6\bullet})_2]^g$	CH_2Cl_2	Mn	(IV)	16.32	[70]
$[Mn^{IV}(L_A^7)(L^{7\bullet})_2]^g$	CH_2Cl_2	Mn	(IV)	15.60	[70]
$[Mn(HL)(H_2O)_3](NO_3)_2\cdot(H_2O)]^h$	MeOH	Mn	(II)	2160.00	[71]
$[Mn(HL)(SCN)_2(H_2O)]\cdot 0.5H_2O]^h$	MeOH	Mn	(II)	1440.00	[71]
$[Mn(HL)(N(CN)_2)(H_2O)_2](NO_3)\cdot H_2O]^h$	MeOH	Mn	(II)	720.00	[71]
$[Zn_2(H_2L^1)(OH)(H_2O)(NO_3)](NO_3)_3]^d$	MeOH	Zn	(II)	1060.00	[72]
$[Zn_2L^2Cl_3]^d$	MeOH	Zn	(II)	882.00	[72]
$[Zn_2L^3Cl_3]^d$	MeOH	Zn	(II)	297.00	[72]
$[Zn_2(L^4)_2(CH_3COO)_2]^d$	MeOH	Zn	(II)	352.00	[72]

L^1 = 2-[(2-piperazin-1-ylethylimino)-methyl]phenol [b] $L2^2$ = 2,6-bis(R-iminomethyl)-4-methyl-phenolato, R = N-ethylpiperazine; $L1^4$ = 2-formyl-4-methyl-6R-iminomethyl-phenolato, R = N-ethylmorpholine; $L1^1$ = 2-formyl-4-methyl-6R-iminomethyl-phenolato. R = N-propylmorpholine; $L2^3$ = 2,6-bis(R-iminomethyl)-4-methyl-phenolato, R = N-ethylpyrrolidine; $L2^1$ = 2,6-bis(R-iminomethyl)-4-methyl-phenolato; R = N-propylmorpholine. [c] $L1^1$ = 2,6-bis(R-iminomethyl)-4-chloro-phenolato, R = N-ethylpiperidine; $L1^2$ = 2,6-bis(R-iminomethyl)-4-t-butyl-phenolato, R = N-ethylpiperidine; $L2^1$ = 2-formyl-4-methyl-6R-iminomethyl-phenolato, R = N-ethylpiperidine; $L1^3$ = 2,6-bis(R-iminomethyl)-4-chloro-phenolato, R = N-ethylmorpholine; $L1^4$ = 2,6-bis(R-iminomethyl)-4-t-butyl-phenolato, R = N-ethylmorpholine; $L1^5$ = 2,6-bis(R-iminomethyl)-4-chloro-phenolato, R = N-propylmorpholine; $L1^6$ = 2,6-bis(R-iminomethyl)-4-t-butyl-phenolato, R = N-propylmorpholine; $L1^7$ = 2,6-bis(R-iminomethyl)-4-chloro-phenolato, R = N-ethylpyrrolidine; $L1^9$ = 2,6-bis(R-iminomethyl)-4-t-butyl-phenolato, R = N-ethylpyrrolidine; $L1^{10}$ = 2,6-bis(R-iminomethyl)-4-chloro-phenolato, R = N-ethylpiperazine; $L1^{12}$ = 2,6-bis(R-iminomethyl)-4-t-butyl-phenolato, R = N-ethylpiperazine. [d] L1 = 2,6-bis(R-iminomethyl)-4-methyl-phenolato, R = N-ethylpiperazine; L2 = 2,6-bis(R-iminomethyl)-4-methyl-phenolato, R = N-ethylpyridine; L3 = 2,6-bis(R-iminomethyl)-4-methyl-phenolato, R = N-ethylpyrrolidine; L4 = 2,6-bis(R-iminomethyl)-4-methyl-phenolato, R = benzylamine. [e] L^1 = 2,7-bis(2-hydroxyphenyl)-2,6-diazaocta-2,6-diene; L^2 = 1,7-bis(2-hydroxyphenyl)-2,6-diazahepta-1,6-diene). [f] L^2 = N,N′-1-methylethylenebis(3-formyl-5-methylsalicylaldimine); L^3 = N,N′-1,1-dimethylethylenebis(3-formyl-5-methylsalicylaldimine); L^4 = N,N′-cyclohexenebis(3-formyl-5-methylsalicylaldimine). [g] L^1 = 1,3-bis(4,6-di-tert-butyl-2-iminophenol)benzene; L^2 = 2-anilino-4,6-di-tert-butylphenol; L^3 = 2-(3,5-di t-butyl-anilino)-4,6-di-tert-butylphenol; L^4 = 2-(3,5-di-trifluromethane-anilino)-4,6-di-tert-butylphenol; L^5 = 2-(3,5-di methyl-anilino)-4,6-di-tert-butylphenol; L^6 = 2-(3,5-di chloro-anilino)-4,6-di-tert-butylphenol; L^7 = 2-(3,5-di methoxy-anilino)-4,6-di-tert-butylphenol. [h] HL = 2,6-bis{2-(N-ethyl)pyridineiminomethyl}-4-methylphenolato.

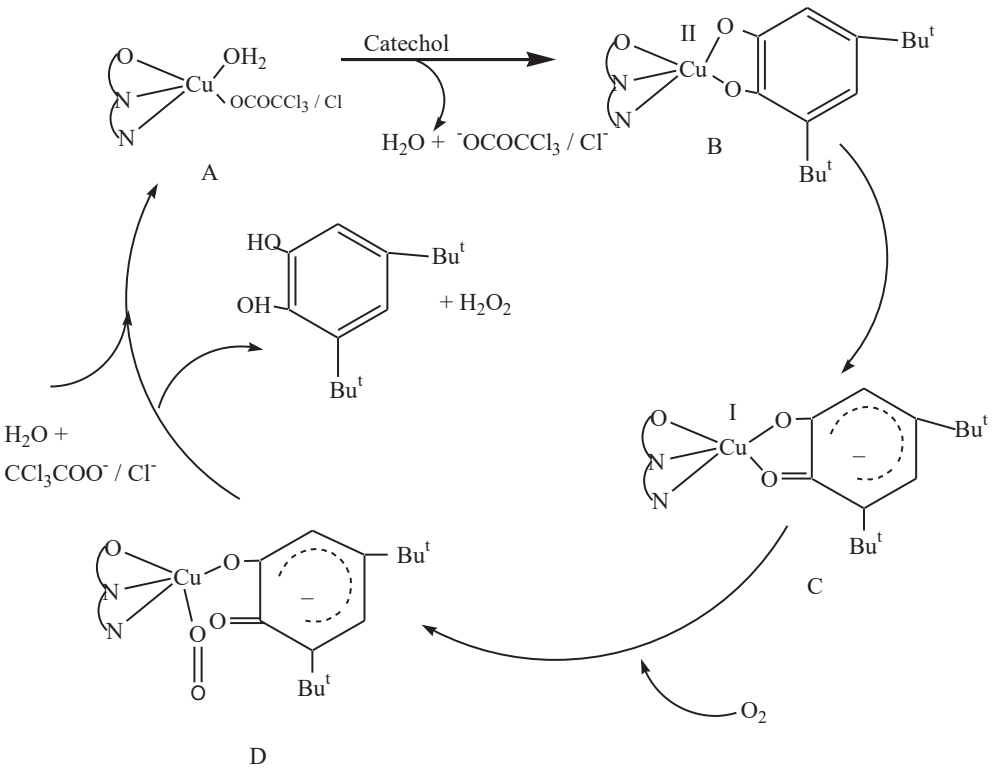

Scheme 4. A plausible mechanistic pathway for aerobic oxidation of catechol by complex **1** or complex **2**.

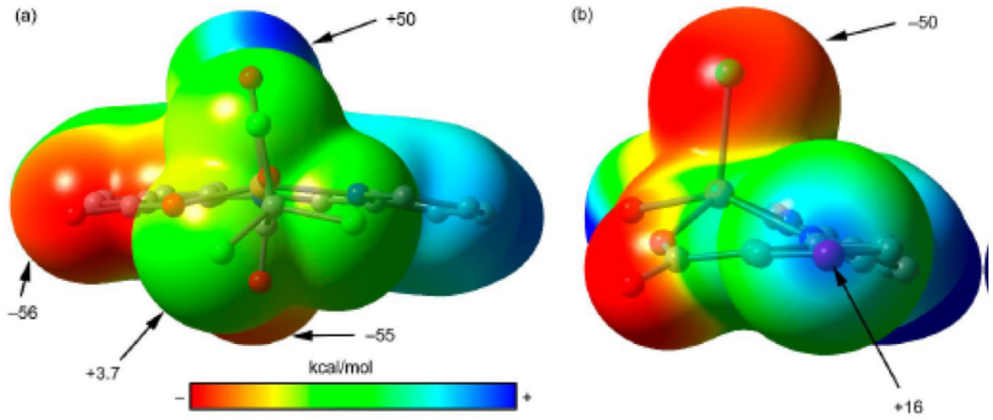

Fig. 15. MEP surface plots (isosurface 0.001 a.u.) of compounds **1** (a) and **2** (b). The MEP values at selected points of the surface are indicated in kcal/mol.

halogen bonding interaction.

Fig. 16b and c shows two self-assembled dimers observed in the solid state of compound **2**. In the dimer involving Cu2 complex (Fig. 16 b), the symmetrically equivalent halogen bonds implicate the chlorido ligand (C—I···Cl) and in the dimer involving Cu1, the carboxylate instead of Cl participates in the halogen bonds (C—I···O). The later are less directional than the former, which is likely related with the stronger interaction obtained for the C—I···Cl bonds ($\Delta E_3 = -10.2$ kcal/mol) compared to C—I···O bonds ($\Delta E_3 = -6.0$ kcal/mol).In order to further characterize the halogen bonding interactions, we have used the NCIplot index. This index and its associated isosurfaces allow to identify which regions of a supramolecular complex interact easily. The non-covalent contacts are revealed with the regions of small reduced density gradient (s) at low densities. These regions are plotted by using an isosurface of s for a low value of density (ρ). In addition, the isosurfaces are coloured using red-yellow-red-blue color code according to values of ρ, where yellow and red correspond to weak and strongly repulsive interactions, respectively, and green and blue are used for weak and strongly attractive interactions, respectively. For a more detailed description of NCI, see theoretical methods. The NCI plot of compound **1** is given in Fig. 16d. It can be observed that each halogen bond is characterized by a green (attractive) isosurface located between the non-coordinated O-atom of trichloroacetate and the Cl—atom belonging to the trichloroacetate of the neighboring molecule. The NCI plot also shows a green surface between the O-atom os the carboxylate group and the H-atoms of the coordinated water molecule, thus confirming the existence of the long H-bond. The NCI plot of the self-assembled dimers of compound **2** are represented in Fig. 16e and f. In both cases the

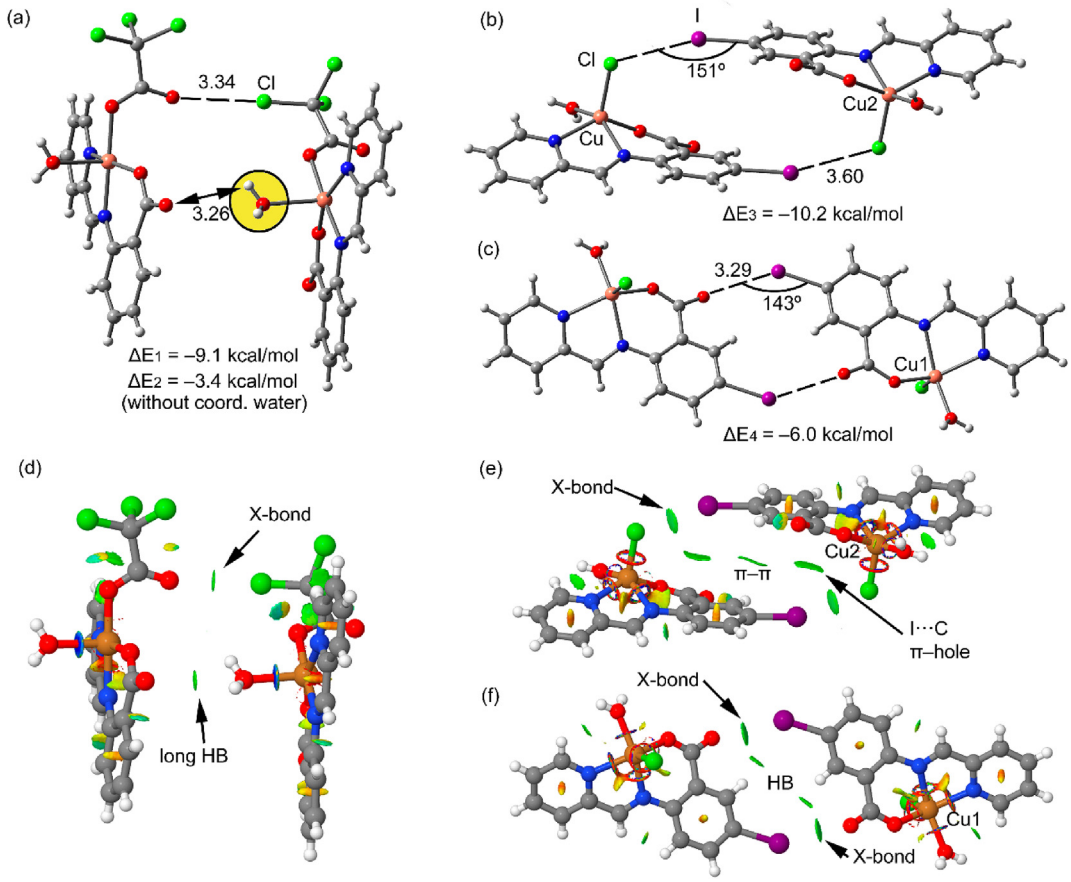

Fig. 16. (a) Dimer of compound **1** retrieved from the X-ray structure. (b) X-ray structure of the self-assembled dimer of compound **2** corresponding to the Cu2 complex. (c) X-ray structure of the self-assembled dimer of compound **2** corresponding to the Cu1 complex. The interactions energies at the B3LYP-D3/def2-TZVP level of theory are also indicated. Distances in Å. (**d-f**) NCI surfaces of the halogen bonding complexes in **1** (d) and **2** (e,f). The gradient cut-off is s = 0.35 au, and the color scale is $-0.04 < \rho < 0.04$ au.

existence of the halogen bonds is confirmed by the presence of small and green isosurfaces located between the I atoms and either the Cl (Fig. 16e) or O (Fig. 16f). Moreover, in both dimers the NC Iplot reveals the existence of other interactions that also contribute to the formation of the dimers. Remarkably, in the dimer of Cu2 complex (Fig. 16e), the belt of the I-atom interacts with the C-atom of the coordinated carboxylate group, thus establishing a π−hole interaction. In the dimer of Cu1 complex (Fig. 16e, the belt of I interacts with an aromatic H-atom located between the I and carboxylate substituents of the ring.

4. Concluding remarks

We have synthesized and X-ray characterized two new Cu(II) complexes with Schiff base ligands derived from anthranilic acid and 4-iodo-anthranilic acid. Both compounds exhibit catecholase activity and we have shown their effectiveness towards the aerial oxidation of 3,5-di-tert-butyl catechol to the corresponding quinine in both DMSO and THF medium. Interestingly, both compounds form dimers in the solid state governed by halogen bonding interactions, which have been characterized energetically (ranging from −3 to −5 kcal/mol) by DFT calculations and also using the NCI plot computational tool.

Declaration of competing interest

There are no conflicts of interest to declare.

CRediT authorship contribution statement

Barun Kumar Biswas: Conceptualization, Methodology. **Sandeepta Saha:** Writing - original draft. **Niladri Biswas:** Software, Validation, Data curation. **Manas Chowdhury:** Data curation, Writing - review & editing. **Antonio Frontera:** Formal analysis, Software, Validation. **Corrado Rizzoli:** Visualization, Investigation, Software. **Ruma Roy Choudhury:** Writing - review & editing. **Chirantan Roy Choudhury:** Supervision, Project administration.

Acknowledgements

C. Roy Choudhury acknowledge DST- FIST (Project No. SR/FST/CSI-246/2012) New Delhi, Govt. of India for instrumental support under capital heads.

Appendix A. Supplementary data

Supplementary data to this article can be found online at https://doi.org/10.1016/j.molstruc.2020.128398.

References

[1] R. Sanyal, P. Kundu, E. Rychagova, G. Zhigulin, S. Ketkov, B. Ghosh, S.K. Chattopadhyay, E. Zangrando, D. Das, New J. Chem. 40 (2016) 6623.
[2] A. Hazari, L.K. Das, R.M. Kadam, A. Bauza, A. Frontera, A. Ghosh, Dalton Trans. 44 (2015) 3862.
[3] Y. Manojkumar, S. Ambika, R. Arulkumar, B. Gowdhami, P. Balaji, G. Vignesh, S. Arunachalam, P. Venuvamalingam, R. Thirumurugan, M.A. Akbarsha, New J.

Chem. 43 (2019) 11391.
[4] A. Bhattacharjee, S. Halder, K. Ghosh, C. Rizzoli, P. Roy, New J. Chem. 41 (2017) 5696.
[5] M. Hazra, T. Dolui, A. Pandey, S.K. Dey, A. Patra, J. Saudi Chem. Soc. 21 (2017) 5240.
[6] M. Shyamal, T.K. Mondal, A. Panja, A. Saha, RSC Adv. 4 (2014) 53520.
[7] T. Klabunde, C. Eicken, J.C. Sacchettini, B. Krebs, Nat. Struct. Biol. 5 (1998) 1084.
[8] N.A. Rey, A. Neves, A.J.C.T. Bortoluzzi, C.T. Pich, H. Terenzi, Inorg. Chem. 46 (2007) 348.
[9] C. Belle, C. Beguin, I. Gautier-Luneau, S. Hamman, C. Philouze, J.L. Pierre, F. Thomas, S. Torelli, Inorg. Chem. 41 (2002) 479.
[10] J. Anekwea, A. Hammerschmidta, A. Rompelb, B. Krebs, Z. Anorg. Allg. Chem. 632 (2006) 1057.
[11] J. Ackermann, F. Meyer, E. Kaifer, H. Pritzkow, Chem. Eur J. 8 (2002) 247.
[12] J. Mukherjee, R. Mukherjee, Inorg. Chim. Acta. 337 (2002) 429.
[13] M. Merkel, N. Mçller, M. Piacenza, S. Grimme, A. Rompel, B. Krebs, Chem. Eur J. 11 (2005) 1201.
[14] C. Fernandes, A. Neves, J. Bortoluzzi, A.S. Mangrich, E. Rentschler, B. Szpoganicz, E. Schwingel, Inorg. Chim. Acta. 320 (2001) 12.
[15] A. Neves, L.M. Rossi, A.J. Bortoluzzi, A.S. Mangrich, W. Haase, R. Werner, J. Braz. Chem. Soc. 12 (2001) 747.
[16] P.K. Nanda, V. Bertolasi, G. Aromí, D. Ray, Polyhedron 27 (2009) 987.
[17] R. Gupta, S. Mukherjee, R. Mukherjee, Polyhedron 19 (2000) 1429.
[18] A. Majumder, S. Goswami, S.R. Batten, M.S. El Fallah, J. Ribas, S. Mitra, Inorg. Chim. Acta. 359 (2006) 2375.
[19] C.-H. Kao, H.-H. Wei, Y.-H. Liu, G.-H. Lee, Y. Wang, C.-J. Lee, J. Inorg. Biochem. 84 (2001) 171.
[20] M. Thirumavalavan, P. Akilan, M. Kandaswamy, G. Chinnakali, G. Senthil Kumar, H.K. Fun, Inorg. Chem. 42 (2003) 3308.
[21] S.J. Smith, C.J. Noble, R.C. Palmer, G.R. Hanson, G. Schenk, L.R. Gahan, M. Riley, J. Biol. Inorg. Chem. 13 (2008) 499.
[22] E.I. Solomon, U.M. Sundaram, T.E. Machonkin, Chem. Rev. 96 (1996) 2563.
[23] N. Kitajima, Y. Moro-oka, Chem. Rev. 94 (1994) 737.
[24] C. Eicken, B. Krebs, J.C. Sacchettini, Curr. Opin. Struct. Biol. 9 (1999) 677.
[25] (a) A. Martinez, I. Membrillo, V.M. Ugalde-Saldivar, L. Gasque, J. Phys. Chem. B116 (2012) 8038;
(b) B. Sreenivasulu, Aust. J. Chem. 62 (2009) 968;
(c) L. Gasque, V.M. Ugalde-Saldivar, I. Membrillo, J. Olguin, E. Mijangos, S. Bernes, I. Gonzalez, J. Inorg. Biochem. 102 (2008) 1227;
(d) A. Banerjee, S. Sarkar, D. Chopra, E. Colacio, K.K. Rajak, Inorg. Chem. 47 (2008) 4023;
(e) I.A. Koval, D. Pursche, A.F. Stassen, P. Gamez, B. Krebs, Jan Reedijk, Eur. J. Inorg. Chem. (2003) 1669;
(f) I.A. Koval, M. Huisman, A.F. Stassen, P. Gamez, O. Roubeau, C. Belle, J.L. Pierre, E. Saint-Aman, M. Lüken, B. Krebs, M. Lutz, A.L. Spek, J. Reedijk, Eur. J. Inorg. Chem. (2004) 4036.
[26] (a) A.L. Abuhijleh, J. Pollitte, C. Woods, Inorg. Chim. Acta. 215 (1994) 131;
(b) A.L. Abuhijleh, C. Woods, E. Bogas, G.L. Guenniou, Inorg. Chim. Acta. 195 (1992) 67;
(c) M.R. Malachowski, M.G. Davidson, J.N. Hoffman, Inorg. Chim. Acta. 157 (1989) 91;
d) M.R. Malachowski, M.G. Davidson, Inorg. Chim. Acta. 162 (1989) 199;
(e) M. Mitra, A.K. Maji, B.K. Ghosh, G. Kaur, A.R. Choudhury, C.-H. Lin, J. Ribas, R. Ghosh, Polyhedron 61 (2013) 15.
[27] B. Mandal, M.C. Majee, T. Rakshit, S. Banerjee, P. Mitra, D. Mandal, J. Mol. Struct. 1193 (2019) 265.
[28] S. Adhikari, A. Banerjee, S. Nandi, M. Fondo, J. Sanmartín-Matalobos, D. Das, RSC Adv. 5 (2015) 10987.
[29] M.K. Panda, Mobin M. Shaikh, R.J. Butcher, P. Ghosh, Inorg. Chim. Acta. 372 (2011) 145.
[30] S. Caglara, I.E. Aydemira, E. Adıgüzela, B. Caglara, S. Demirb, O. Buyukgungo, Inorg. Chim. Acta. 408 (2013) 131.
[31] A. Neves, L.M. Rossi, A.J. Bortoluzzi, B. Szpoganicz, C. Wiezbicki, E. Schwingel, Inorg. Chem. 41 (2002) 1788.
[32] S. Mandal, M. Chakraborty, A. Mondal, B. Pakhira, A.J. Blake, E. Sinn, S.K. Chattopadhyay, New J. Chem. 42 (2018) 9588.
[33] K. Valegard, A.C.T. Van Scheltinga, M.D. Lloyd, T. Hara, S. Ramaswamy, A. Perrakis, A. Thompson, H.J. Lee, J.E. Baldwin, C.J. Schofield, J. Hajdu, I. Andersson, Nature 394 (1998) 805.
[34] M.J. Gajewska, Ching Wei-Min, Y.-S. Wen, C.-H. Hung, Dalton Trans. 43 (2014) 14726.
[35] T. Campbell, F. Urbach, Inorg. Chem. 12 (1973) 1836.
[36] W. Potter, L. Taylor, Inorg. Chem. 15 (1976) 1329.
[37] A.N. Vlček, Coord. Chem. Rev. 230 (2002) 225.
[38] J. Garcıá-Tojal, T. Rojo, Polyhedron 18 (1999) 1123.
[39] J. Garcıá-Tojal, A. Garcıá-Orad, A.A. Dıaz, J.L. Serra, M.K. Urtiaga, M.A.I. Arriortua, T. Rojo, J. Inorg. Biochem. 84 (2001) 271.
[40] M. Shakir, M. Azam, Y. Azim, S. Parveen, A.U. Khan, Polyhedron 26 (2007) 5513.
[41] M. Boča, D. Valigura, W. Linert, Tetrahedron 56 (2000) 441.
[42] F.A. French, E.J. Blanz Jr., J. Med. Chem. 9 (1966) 585.
[43] A.H. Mirza, M.H.S.A. Hamid, S. Aripin, M.R. Karim, M. Arifuzzaman, M.A. Ali, P.V. Bernhardt, Polyhedron 74 (2014) 16.
[44] C.-J. Qiu, Y.-C. Zhang, Y. Gao, J.-Q. Zhao, J. Organomet. Chem. 694 (2009) 3418.
[45] X.-B. Yang, Y. Huang, J.-S. Zhang, S.-K. Yuan, R.-Q. Zeng, Inorg. Chem. Commun. 13 (2010) 1421.
[46] C.-M. Liu, R.-G. Xiong, X.-Z. You, Y.-J. Liu, K.-K. Cheung, Polyhedron 15 (1996) 4565.
[47] A. Sasmal, E. Garribba, C. Rizzoli, S. Mitra, Inorg. Chem. 53 (2014) 6665.
[48] Qian Shi, Rongcao, Mao Chun Hong, Yao Yu Wang, QiZhen Shi, Trans. Met. Chem. 26 (2001) 657.
[49] Bruker, *APEX2,SAINT* and *SADABS*, Bruker AXS Inc., Madison, WI, USA, 2008.
[50] (a) G.M. Sheldrick, SHELXT-integrated space-group and crystal-structure determination, Acta Crystallogr. A71 (2015) 3–8;
(b) G.M. Sheldrick, Crystal structure refinement with SHELXL, Acta Crystallogr. C71 (2015) 3–8.
[51] (a) O.V. Dolomanov, L.J. Bourhis, R.J. Gildea, J.A.K. Howard, H. Puschmann, OLEX2: a complete structure solution, refinement and analysis program, J. Appl. Crystallogr. 42 (2009) 339;
(b) Persistence of Vision Pty. Ltd., Persistence of Vision Raytracer [Computer Software], 2004. Retrived from, Version 3.6. http://www.povray.org/download/.
[52] L.J. Farrugia, J. Appl. Crystallogr. 30 (1997) 565.
[53] M.J. Frisch, G.W. Trucks, H.B. Schlegel, G.E. Scuseria, M.A. Robb, J.R. Cheeseman, G. Scalmani, V. Barone, G.A. Petersson, H. Nakatsuji, X. Li, M. Caricato, A.V. Marenich, J. Bloino, B.G. Janesko, R. Gomperts, B. Mennucci, H.P. Hratchian, J.V. Ortiz, A.F. Izmaylov, J.L. Sonnenberg, D. Williams-Young, F. Ding, F. Lipparini, F. Egidi, J. Goings, B. Peng, A. Petrone, T. Henderson, D. Ranasinghe, V.G. Zakrzewski, J. Gao, N. Rega, G. Zheng, W. Liang, M. Hada, M. Ehara, K. Toyota, R. Fukuda, J. Hasegawa, M. Ishida, T. Nakajima, Y. Honda, O. Kitao, H. Nakai, T. Vreven, K. Throssell, J.A. Montgomery Jr., J.E. Peralta, F. Ogliaro, M.J. Bearpark, J.J. Heyd, E.N. Brothers, K.N. Kudin, V.N. Staroverov, T.A. Keith, R. Kobayashi, J. Normand, K. Raghavachari, A.P. Rendell, J.C. Burant, S.S. Iyengar, J. Tomasi, M. Cossi, J.M. Millam, M. Klene, C. Adamo, R. Cammi, J.W. Ochterski, R.L. Martin, K. Morokuma, O. Farkas, J.B. Foresman, D.J. Fox, Gaussian 16, Revision A.03, Gaussian, Inc., Wallingford CT, 2016.
[54] S.F. Boys, F. Bernardi, Mol. Phys. 19 (1970) 553.
[55] J. Contreras-García, E.R. Johnson, S. Keinan, R. Chaudret, J.P. Piquemal, D.N. Beratan, W. Yang, J. Chem. Theor. Comput. 7 (2011) 625.
[56] A. Majeed, K. Al-Sammarrae, N. Salih, J. Salimon, B. Abdullah, Arab. J. Chem. 10 (2017) 1639.
[57] M. Shebl, J. Mol. Struct. 1128 (2017) 79.
[58] M. Shebl, S.M.E. Khalil, S.A. Ahmed, H.A.A. Medien, J. Mol. Struct. 980 (2010) 39.
[59] M.M. Hassanien, I.M. Gabr, M.H. Abdel-Rhman, A.A. El-Asmy, Spectrochim. Acta A 71 (2008) 73.
[60] M. Shyamal, T.K. Mandal, A. Panja, A. Saha, RSC Adv. 4 (2014) 53520.
[61] A.W. Addison, T.N. Rao, J. Reedijk, J. van Rijn, G.C. Verschoor, J. Chem, Soc, Dalton Trans. (1984) 1349.
[62] N. Biswas, S. Saha, S. Khanra, A. Sarkar, D.P. Mandal, S. Bhattacharjee, A. Chaudhuri, S. Chakraborty, C.R. Choudhury, J. Biomol. Struct. Dyn. 37 (2018) 2801.
[63] S. Saha, N. Biswas, A. Sasmal, C.J. Gómez-García, E. Garribba, A. Bauza, A. Frontera, G. Pilet, G.M. Rosair, S. Mitra, C.R. Choudhury, Dalton Trans. 47 (2018) 16102.
[64] (a) S. Saha, C.R. Choudhury, G. Pilet, A. Frontera, S. Mitra, J. Coord. Chem. 70 (2017) 1389;
(b) S. Saha, A. Sasmal, C.R. Choudhury, C.J. Gómez-Garcia, E. Garribba, S. Mitra, Polyhedron 69 (2014) 262.
[65] A.K. Ghosh, M. Mitra, A. Fathima, H. Yadav, A. Roy Choudhury, B.U. Nair, R. Ghosh, Polyhedron 107 (2016) 1.
[66] P. Chakraborty, I. Majumder, K.S. Banu, B. Ghosh, H. Kara, E. Zangrando, D. Das, Dalton Trans. 45 (2016) 742.
[67] C.T. Yang, M. Vetrichelvan, X. Yang, B. Moubaraki, K.S. Murray, J.J. Vittal, Dalton Trans. (2004) 113.
[68] Y. Thio, X. Yang, J.J. Vittal, Dalton Trans. 43 (2014) 3545.
[69] J. Reim, B. Krebs, J. Chem. Soc., Dalton Trans. (1997) 3793.
[70] S. Torelli, C. Belle, I. Gautier-Luneau, J.L. Pierre, E. SaintAman, J.M. Latour, L. Le Pape, D. Luneau, Inorg. Chem. 39 (2000) 3526.
[71] A. Neves, L.M. Rossi, A.J. Bortoluzzi, B. Szpoganicz, C. Wiezbicki, E. Schwingel, Inorg. Chem. 41 (2002) 1788.
[72] K.S. Banu, T. Chattopadhyay, A. Banerjee, S. Bhattacharya, E. Suresh, M. Nethaji, E. Zangrando, D. Das, Inorg. Chem. 47 (2008) 7083.
[73] P. Chakraborty, J. Adhikary, B. Ghosh, R. Sanyal, S.K. Chattopadhyay, A. Bauzá, A. Frontera, E. Zangrando, D. Das, Inorg. Chem. 53 (2014) 8257.
[74] J. Mukherjee, R. Mukherjee, Inorg. Chim. Acta. 337 (2002) 429.
[75] J. Adhikary, P. Chakraborty, S. Das, T. Chattopadhyay, A. Bauzá, S.K. Chattopadhyay, B. Ghosh, F.A. Mautner, A. Frontera, D. Das, Inorg. Chem. 52 (2013) 13442.
[76] (a) P. Seth, M.G.B. Drew, A. Ghosh, J. Mol. Catal. Chem. 365 (2012) 154;
(b) K.S. Banu, T. Chattopadhyay, A. Banerjee, M. Mukherjee, S. Bhattacharya, G.K. Patra, E. Zangrando, D. Das, Dalton Trans. (2009) 8755.
[77] S. Mukherjee, T. Weyhermüller, E. Bothe, K. Wieghardt, P. Chaudhuri, Dalton Trans. (2004) 3842.
[78] A. Guha, K.S. Banu, A. Banerjee, T. Ghosh, S. Bhattacharya, E. Zangrando, D. Das, J. Mol. Catal. Chem. 338 (2011) 51.
[79] A. Guha, T. Chattopadhyay, N.D. Paul, M. Mukherjee, S. Goswami, T.K. Mondal, E. Zangrando, D. Das, Inorg. Chem. 51 (2012) 8750.
[80] (a) I.A. Koval, P. Gamez, C. Belle, K. Selmeczi, J. Reedijk, Chem. Soc. Rev. 35

(2006) 814;
(b) K. Selmeczi, M. Reglier, M. Giorgi, G. Speier, Coord. Chem. Rev. 245 (2003) 191;
(c) R. Than, A.A. Feldmann, B. Krebs, Coord. Chem. Rev. 182 (1999) 211;
(d) E.I. Solomon, U.M. Sundaram, T.E. Machonkin, Chem. Rev. 96 (1996) 2563;
(e) S.J. Smith, C.J. Noble, R.C. Palmer, G.R. Hanson, G. Schenk, L.R. Gahan, M. Riley, J. Biol. Inorg. Chem. 13 (2008) 499.
[81] (a) J. Ackermann, F. Meyer, E. Kaifer, H. Pritzkow, Chem. Eur J. 8 (2002) 247;
(b) J. Reim, B. Krebs, J. Chem. Soc., Dalton Trans. (1997) 3793.
[82] (a) J. Anekwe, A. Hammerschmidt, A. Rompel, B. Krebs, Z. Anorg. Allg. Chem. 632 (2006) 1057;
(b) V.K. Bhardwaj, N. Aliaga-Alcalde, M. Corbella, G. Hundal, Inorg. Chim. Acta. 363 (2010) 97;
(c) A. Banerjee, R. Singh, E. Colacio, K.K. Rajak, Eur. J. Inorg. Chem. (2009) 277;
(d) N.A. Rey, A. Neves, A.J. Bortoluzzi, C.T. Pich, H. Terenzi, Inorg. Chem. 46 (2007) 348.
[83] (a) C.-H. Kao, H.-H. Wei, Y.-H. Liu, G.-H. Lee, Y. Wang, C.-J. Lee, J. Inorg. Biochem. 84 (2001) 171;
(b) C. Belle, C. Beguin, I. Gautier-Luneau, S. Hamman, C. Philouze, J.L. Pierre, F. Thomas, S. Torelli, Inorg. Chem. 41 (2002) 479.
[84] P. Chakraborty, S. Majumder, A. Jana, S. Mohanta, Inorg. Chim. Acta. 410 (2014) 65.
[85] P. Adak, B. Ghosh, A. Bauzá, A. Frontera, A.J. Blake, M. Corbella, C.D. Mukhopadhyay, S.K. Chattopadhyay, RSC Adv. 6 (2016) 86851.
[86] A. Biswas, K.L. Das, M.G.B. Drew, C. Diaz, A. Ghosh, Inorg. Chem. 51 (2012) 10111.
[87] J. Kaizer, T. Csay, G. Speier, M. Giorgi, J. Mol. Catal. Chem. 329 (2010) 71.
[88] (a) M. Das, R. Nasani, M. Saha, S.M. Mobin, S. Mukhopadhyay, Dalton Trans. 44 (2015) 2299;
(b) A.I. Vogel, A Text Book of Quantitative Inorganic Analysis, third ed., Wiley, New York, 1961, p. 343.